RUNNER SYSTEMS CONTAINING CERAMIC FOAM FILTERS QUANTIFIED BY "AREA NORMALIZED" BIFILM INDEX MAP

Fu-Yuan Hsu, Cheng-Lung Li
National United University, Miaoli City, Taiwan, R.O.C.

Abstract

In the runner system design for aluminum gravity castings, ceramic foam filters were used for reducing the velocity of liquid metal to avoid "bifilm" defects resulting from a high gating velocity (over its critical gating velocity). In this study, three types of runner systems incorporating ceramic foam filters were designed. To observe the flow phenomena in these systems, a water analogy experiment in a transparent plastic mold was utilized. To understand the effect of the filters used in these systems, aluminum sand casting experiments were conducted. The defect contents inside the casting samples in the outlet area of filters were measured by remelt Reduced Pressure Test (remelt RPT) and followed by measuring their bulk densities. A new "bifilm" index map, which uses the index values normalized by the metal area without porosity, was proposed. Finally, an optimized runner system with filter was suggested.

Keywords: *ceramic foam filter, runner system design, gravity casting, bifilm defect, model*

Introduction

When gravity casting aluminum alloy castings, bottom gating is normally recommended. However, if the velocity of the flow exceeds the critical gating velocity of 0.5 m/s, the metal is likely to enter the mold cavity in the form of a fountain.[1] The turbulence resulting from this mode of flow leads to the entrapment of air and oxide films in the melt, thereby forming " bifilm" defects in the casting.[2] Campbell suggested that the safe range of the critical gating velocity for aluminum casting is between 0.25 and 0.5 m/s.[3] A reliable casting could be produced if the gating velocity were controlled under 0.5 m/s.[4] Therefore, an important aspect of a good runner system design is to control the ingate velocity below this critical value.

In the compact space of a runner system in gravity casting, ceramic foam filters are often applied to reduce the velocity of the flow as a result of the relatively high drag from the reticulated structure of the foam filter and its fine tortuous channels. In view of its potential importance to a filling system design, it is perhaps surprising that more work has not been carried out to study the detailed action of filters on the quality of the castings. The relatively few studies include:

- Sirrell and Campbell[5] noticed that the use of ceramic foam filters in the running system were found to increase the reliability of the cast alloy, apparently through the control of the metal velocity and not through the removal of inclusions from the liquid metal.
- Because it is difficult to observe the flow in the sand mold, Hashemi and Raiszadeh[6] removed the cope of a sand mold and observed the liquid metal flow emerging from the filter.
- To gather more information of the flow going through foam filters, Gebelin and Jolly[7] use the computational modeling to simulate the flow through a filter. They found the temperature distribution in the region of the runner and the filter depended on the design of the runner system.
- Hsu and Lin[8] found that the design of the orientation of the filter incorporating with the runner is very important to achieve a high flow rate but low velocity.
- Din et al.[9] found that 90% of the action of the filter to improve direct pour Al alloy castings was the result of the flow, and only 10% due to any filtering action.

Therefore, the purpose of this study is to explore the further development of the runner system design integrated with the ceramic foam to produce a reliable casting. The observation of the flow filling in the filter and the runner was achieved with a water analogy experiment and the quality of the casting was established with an aluminum casting experiment using identical geometry. The defect content of the casting samples was measured by the remelt Reduced Pressure Test (remelt RPT).

Method

In this study, three runner systems of different shape configurations (L-, U- and J-shaped) incorporating foam filters were designed as shown in Figure 1. In these systems, various total head heights (H) (300, 400 & 600mm) with

or without silicon carbide ceramic foam filters were used. There were two grades of foam filters, 10 ppi (pores per inch) and 20 ppi used.

To observe the filling profile of the flow after the foam filter in these three runner systems, a water analogy experiment was carried out in a transparent plastic mold. To assess any differences in the casting quality from the three runner systems, identical geometries of filling systems were used in sand molds from which aluminum sand castings were produced. The defect content in the castings on the outlet side of the filter was measured by the Reduced Pressure Test (RPT) method, followed by bulk density measurement.

Runner System Design

Figure 1 shows three runner systems. The systems have the same dimensions for the pouring basin, the downsprue and the outlet runner (which in this case effectively forms the casting section). The only difference between the systems is the geometry of the inlet runner before the filter. Various total head height (H), 300, 400 and 600mm, were investigated in all three systems, as being typical of many production castings. Moreover, filterless, 10 & 20 ppi foam filters were designed for these systems. In the pouring basin, a stopper was plugged in the sprue entrance to avoid the premature filling of the downsprue before the liquid level in the basin reached the target head height designed for the runner system. The liquid metal was poured into the pouring basin until the basin was filled to its design level, signaled by the metal overflowing from the basin at which instant the stopper was lifted clear of the basin, permitting the start of filling of the casting. Additional liquid was poured continuously into the basin in order to maintain a constant head height in the basin during the filling of the mold.

The Water Analogy Experiment

Although the flow of metal in the three geometries had been simulated using a commercial fluid dynamics (CFD) package, current computer models of flow cannot simulate the details of jetting and bubble formation which are known to create serious entrainment defects in liquid metals. The overall macroscopic form of the flow in all instances was closely similar in both computer simulated and water models, so that for this experiment, for which details of jetting and bubble formation were required, water modeling was employed. The results of the computer simulations, while in broad detail entirely supportive, are not presented.

Transparent plastic, polymethylmethacrylate (PMMA), was machined to form the shape of the casting as shown in Figure 2. For clear observations, red colored ink was added into the water. The filling sequences of the dyed water were recorded at the speed of 25 frames per second by video camera. Because the kinematic viscosities of aluminum (i.e., 1.27×10^{-6} $m^2 \cdot s^{-1}$) is similar to that of water (i.e., 1.00×10^{-6} $m^2 \cdot s^{-1}$), full-scale water models of runner system for these liquid metals were assumed to give a sufficiently close reproduction of the flow conditions in the actual runner systems.

The Casting Experiment

For the casting experiment the sand mold material was silica sand with a mean particle size of ASTM sieve no. 70~85 mixed with Phenolic-Urethane Cold Box (PUCB) binder at around 1.8% of total sand weight for the combined weight of resin and the curing agent. The sand-resin mixture is compacted against the wood pattern and allowed to cure. Figure 3 shows the sand molds after extraction from the pattern and after assembling. Aluminum alloy, A356 (Al-7%Si-Mg), was melted at 1256 ± 18°F (680 ± 10°C) and degassed with pure argon for two hours. The molten aluminum was then tested by RPT followed by the Archimedes bulk density test.

The metal was then poured at 1292 ± 9°F (700 ± 5°C) into the pouring basin with the ceramic stopper in the sprue entrance until the basin was full, signaled by the molten aluminum overflowing from the basin. Then, the stopper was abruptly lifted clear, permitting the start of filling. Additional mol-

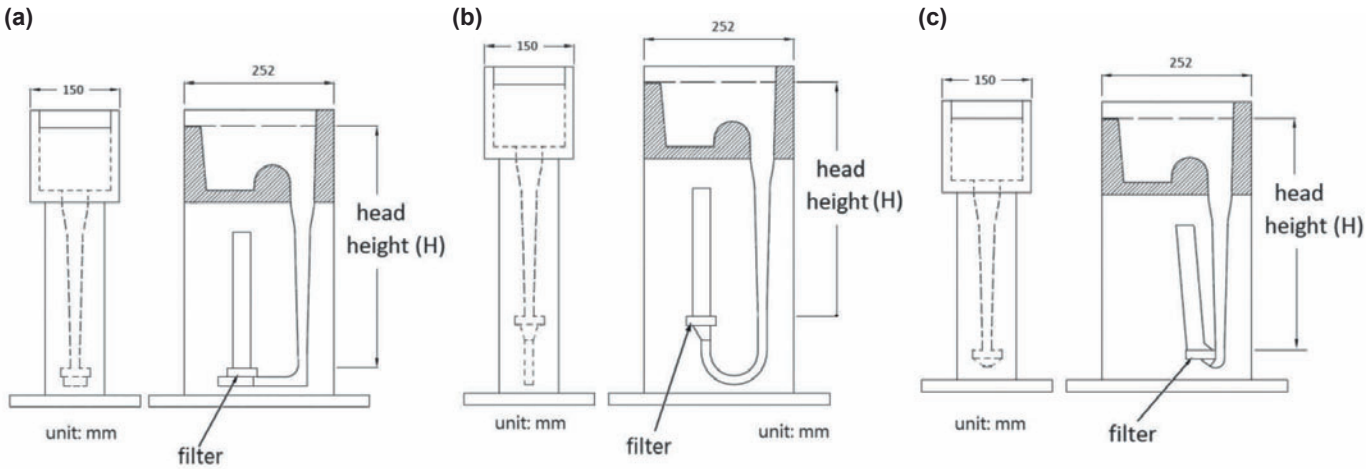

Figure 1. Three runner systems: (a) L- shaped, (b) U- shaped and (c) J- shaped runner systems.

ten aluminum was continuously poured in order to maintain a constant head height in the basin during the filling of the casting. The pouring time was approximately 1~3 seconds depending on the designed head height.

After casting, test samples were cut from the castings in the outlet area of the filter (denoted by the red rectangular region in Figure 4). The sectioned sample was approximately 170g (3cm × 3cm × 7cm) and it was contained in the RPT cup. The cup with the sample was remelted at 1292 ± 9°F (700 ± 5°C) in an electric muffle furnace. The heating procedure was 18°F per min. (10°C per minute). At 1292 ± 9°F (700 ± 5°C) the cup with the remelted sample remained in the furnace for 1 hour before placing under the RPT vacuum. The cup was then transferred from furnace and allowed the remelted sample to re-solidify under vacuum (0.1 atmosphere residual pressures) in the RPT apparatus.

This freezing under reduced pressure opened the bifilms, permitting visualization and measurement. The solidified samples were then sealed with a thin coating of paraffin wax prior to their density measurement procedure using the Archimedes' method. The difference in density between the original melt and the cast samples gave the volume percentage of porosity (ε) in the cast samples.

Bifilm Index Map

To quantify the contents of the bifilm defects in the casting in the outlet area of the foam filter, two measurements of the bifilm index [total length, L (mm) and number N (counts) of bifilms] were derived from the sectioned remelt RPT specimens. In this study, primary continuously cast ingots were used. Thus, it is assumed that number of bifilms would be similar quantity in the original aluminum melt during the melting of these ingots. However, gas contents (mostly hydrogen) in each melt pouring for these casting experiments may be different. Consequently, for standardizing the collected data of the bifilm, new "bifilm" index values, which were L and N respectively normalized by the metal surface area (A_m), were proposed in this study. This area A_m is the surface region without surface porosity on the sectioned remelt RPT samples. Unit area (A_u) is randomly chosen as a squared area of 13mm×13mm on the surface. It is also the area for collecting data for the L and N values. The area of metal surface on the sectioned sample was therefore derived from:

$$A_m = (1- \varepsilon) \times A_u \qquad \text{Eqn. 1}$$

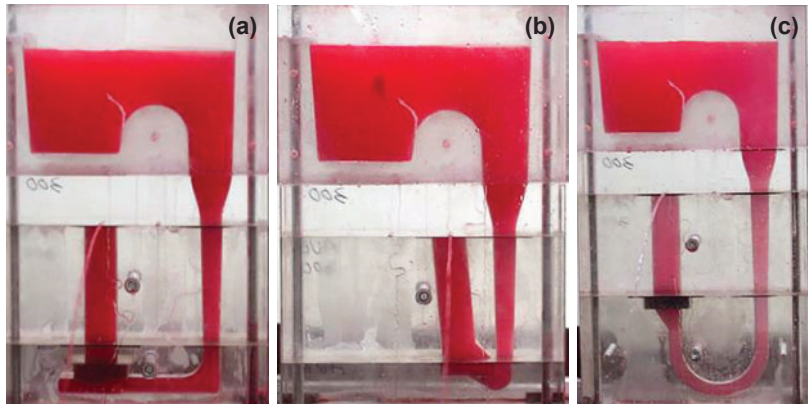

Figure 2. Water analogy experiment: (a) L-, (b) J-, and (c) U- shaped runner systems.

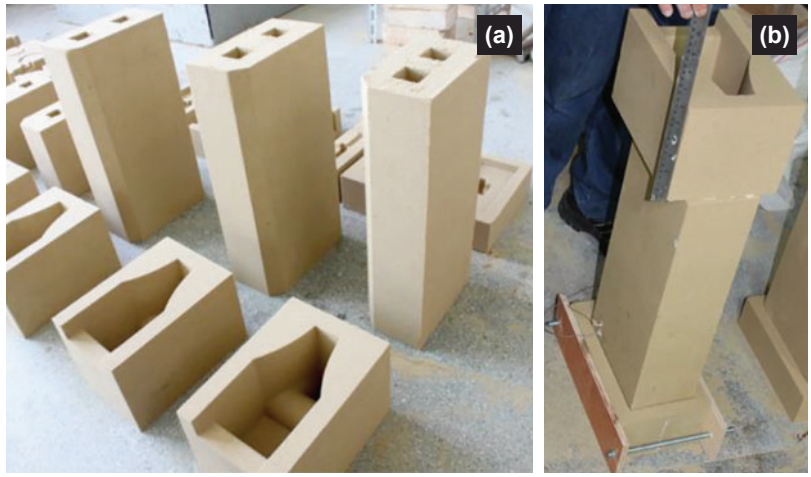

Figure 3. The resin bonded sand mold apparatus, showing: (a) mold parts and (b) the assembled mold.

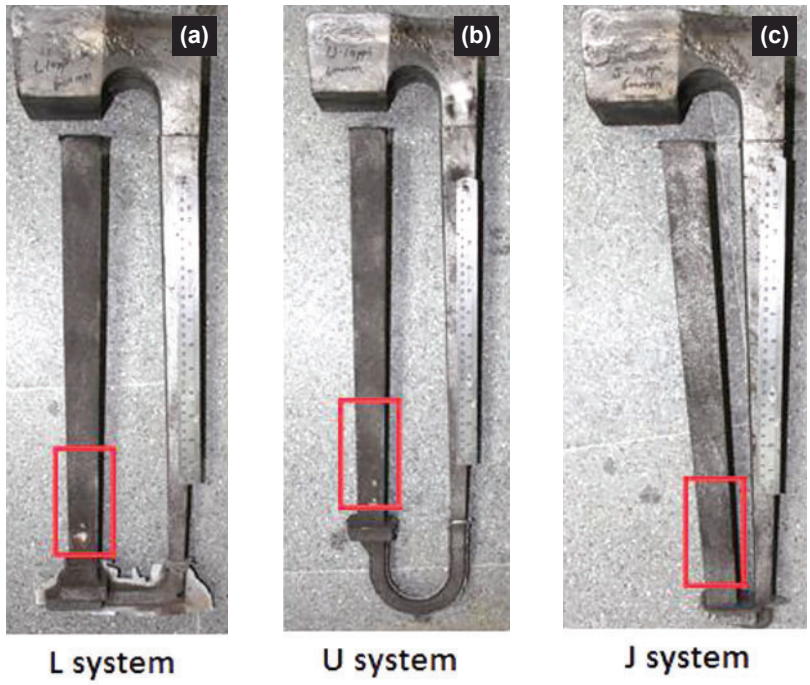

Figure 4. The specimens in the outlet region of the filter for remelt RPT test in (a) L system, (b) U system and (c) J system (indicated by the red square box).

Where; ε is the volume percentage of porosity in a remelt RPT sectioned sample and it is calculated from the density difference between the original degassed solidified melt and the remelt RPT casting sample. As a result, the so-called "area normalized" bifilm index map, which is the L value as function of N value per the metal surface area, could be plotted. The units of the normalized L and N indexes were mm^{-1} and mm^{-2} respectively.

Figure 5 demonstrates the schematic of the same index numbers of L/A_m and N/A_m in two different RPT sectioned samples. For these two samples, their metal surfaces (A_m) were equal regardless of their various porosity volumes. The volume of the porosities (the inflated bifilms) depends on the hydrogen content of the liquid aluminum melt (or humidity conditions) during pouring. It was difficult to control the casting environment in each casting. The hydrogen content in the aluminum melt was therefore random in each casting case. The purpose of designing the "area normalized" bifilm index was to avoid this random hydrogen content condition by eliminating the porosity aspect. The normalized area, metal surface region (A_m) on the sectioned specimens was the real metal surface area without porosity.

Because the index was normalized by the actual metal surface area, the counting of bifilms, their total length and number, within the measured unit area seemed to increase. This result was reasonable since it is closer to the true density of bifilms of the casting samples without porosity volumes.

The assumptions for applying the "area normalized" bifilm index map to quantify bifilms generated in runner systems were:

- First; bifilm development was solely determined by the geometry of runner systems; No other factors influenced the creating of bifilms.
- Second; each casting environment (i.e., humidity, hydrogen content) were ignored by dividing the area A_m. It was actual metal surface area subtracted from porosity volume of RPT samples.
- Third: after the area normalization process, the density of bifilms per actual metal surface area was equal to other castings in the same runner system.

In Figure 5, due to the same index numbers, it was suggested that the two samples come from the same runner system which developed identical quantity (numbers) and quality (total length) of bifilms.

Figure 6 shows the schematic of changing size and number of bifilms as altering index numbers at various changing paths in the "area normalized" bifilm index map. In Path (a), the number of bifilm was constant but size increased; in Path (b) size was constant but the number increased; in Path (c) size became smaller but the total length was constant.

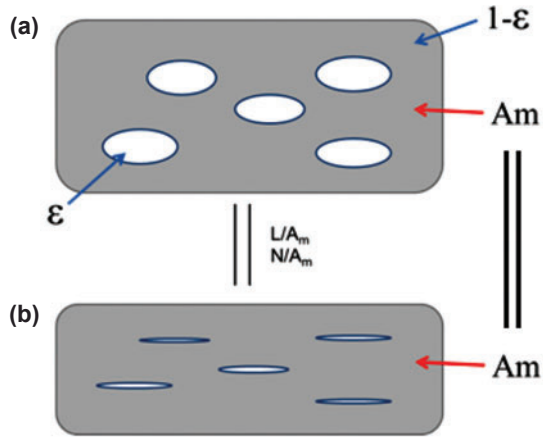

Figure 5. Schematic illustration of two equal bifilms counts per metal surface area A_m: (a) inflated bifilms and (b) flattened bifilms.

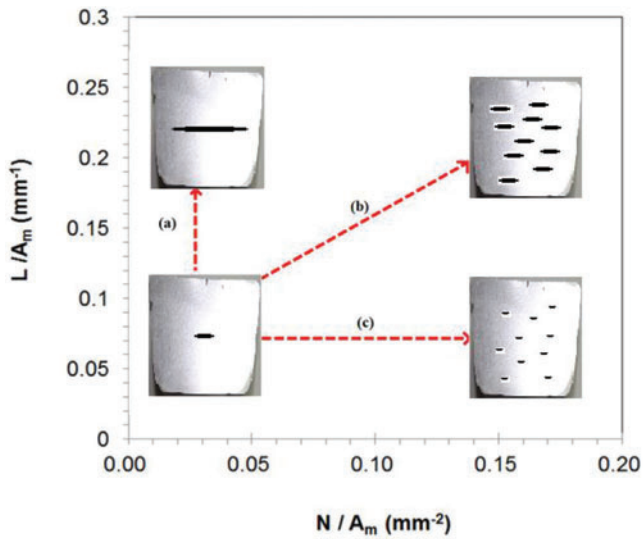

Figure 6. Schematic illustration of the diagram of L/A_m and N/A_m at various changes of index numbers: Path (a) bifilm total length was increased and their number was constant; Path (b) the total length was constant and number was increased; Path (c) the total length was constant and the number was increased.

Results

The result of the observation for the profile of the flow coming out from the filter was shown in the water analogy experiment, while the quality of the casting in the outlet area of the filter was presented in the casting experiment.

Water Analogy Experiment

Figure 7a shows the water profile at various time frames in the filterless L-shaped runner system. At 0.27s, the water began to fill the filter cavity. It gradually filled from the left to the right side of the filter until the filter cavity was filled completely as shown. There is no air entrapment in this runner system during the filling. But the velocity of the flow in the runner is still high.

In Figure 7b, the 10 ppi filter was now included in the L-shaped system. The flow started to fill the filter at 0.27s from the left and progressed to the right side of the filter in the figure. Importantly, the flow is more quiescent and there was no air entrapment in this runner system; the filter was seen to control the velocity of the 'downstream' flow.

Figure 8a shows the water profile at various time frames in the filterless U-shaped runner system. The first jet arrived at the filter cavity at 0.24s from the starting of the pouring. At 0.33s, the jet reached its highest point of 90 ± 5mm from the cavity and subsequently started to fall. After 0.42s, the falling flow entrapped the air in the runner cavity, forming bubbles. At 0.6s, two large bubbles appeared in the runner section.

In Figure 8b the U-shaped system with the 10 ppi filter is shown. The flow jet contacted the filter at 0.30s. This jet continued to impact the underside of the filter until the cavity beneath the filter was completely filled at 0.39s. After 0.42s, the flow emerged from the filter and started to fill the runner cavity. A few incidents of air entrapment were recorded from the jet action under the filter, but after the filter, further entrapment was avoided. The flow emerged relatively quiescently from the filter (Figure 8b).

Figure 9a demonstrates the water profile at various time frames in the filterless J-shaped runner system. The first jet arrived at the filter cavity at 0.30s from the start of pouring. At 0.42s, the jet reached its highest point of 75 ± 5mm from the cavity and subsequently started to fall. After 0.48s, the falling flow entrapped the air in the runner cavity, forming bubbles. At 0.6s, a few bubbles appeared in the cavity.

Figure 9b illustrates the J-shaped system with the 10 ppi filter. The flow jet contacted the filter at 0.30s. This jet continued to impact the underside of the filter until the cavity beneath the filter was completely filled at 0.33s. After 0.33s, the flow emerged from the filter and started to fill the runner cavity. In the filter outlet, the slower jet went toward the

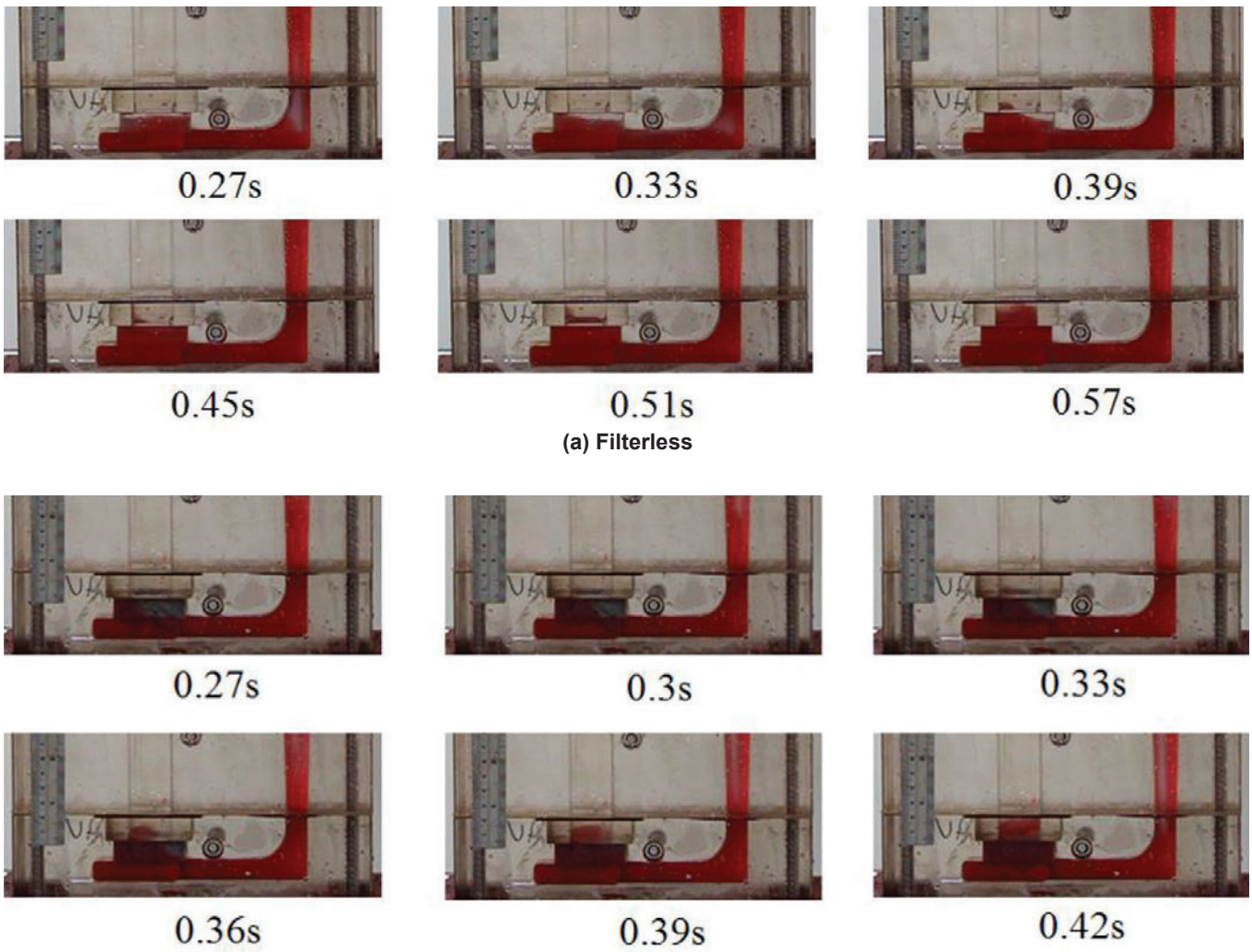

Figure 7. The water experiments for L-shaped runner systems with: (a) filterless and (b) 10 ppi foam filter at the head height of 400mm at various time frames.

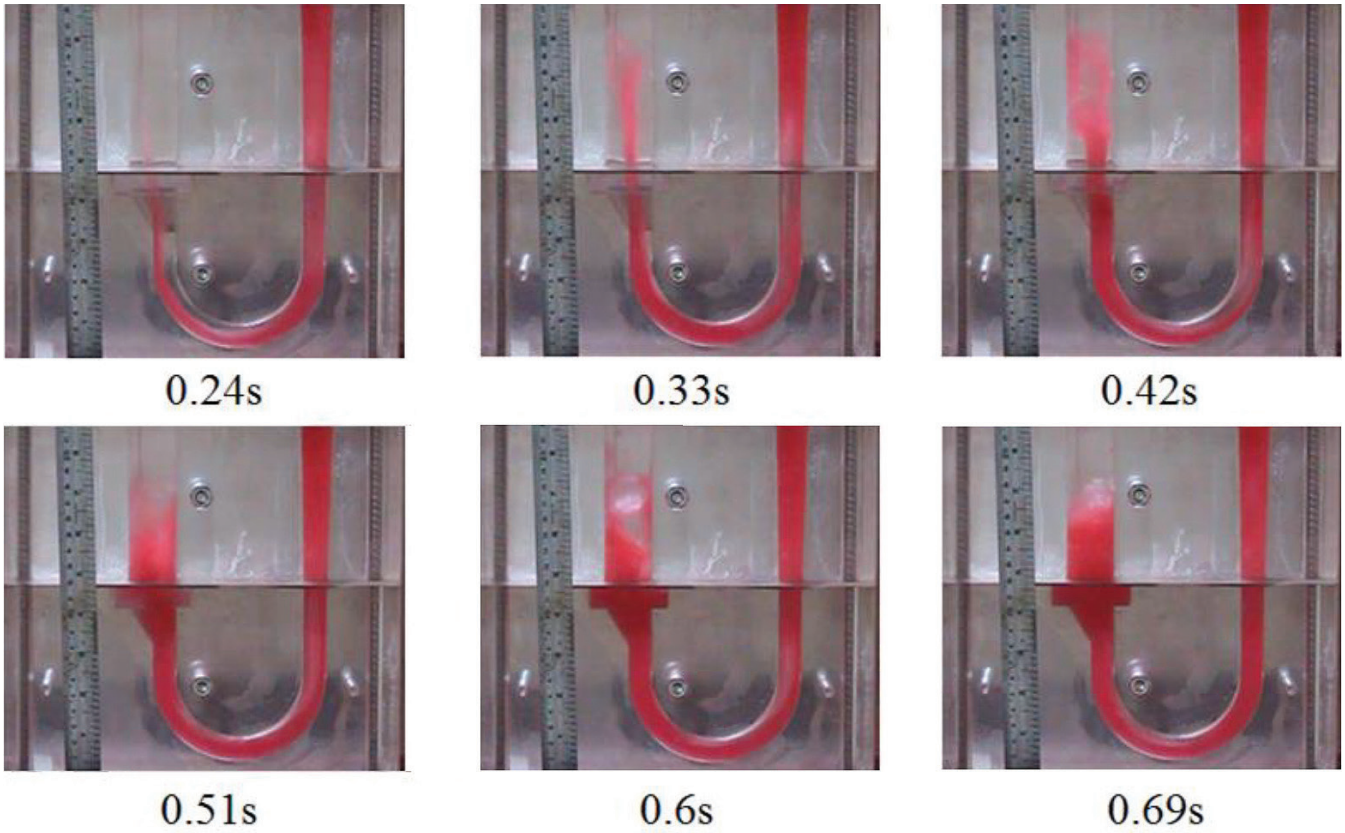

(a) Filterless

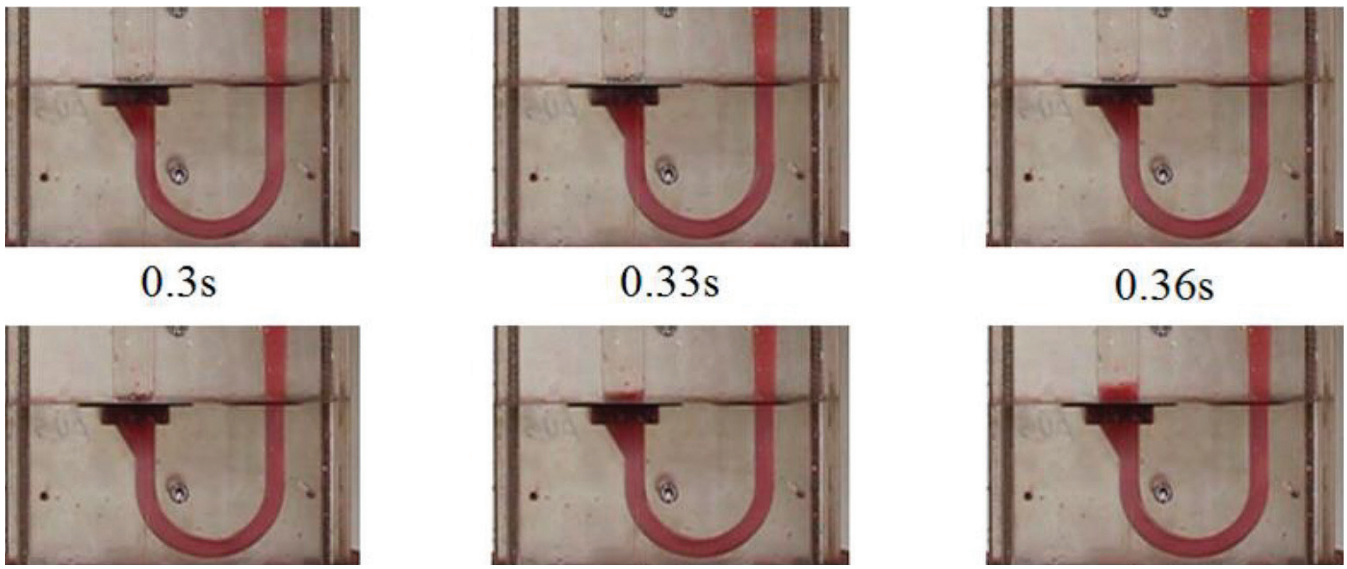

(b) 10 ppi Filter

Figure 8. The water experiments for the U-shaped runner systems with: (a) filterless and (b) 10 ppi foam filter at the head height of 400mm at various time frames.

farther side of the mold cavity. Bubbles were avoided after the filter in this system.

Furthermore, the flow emerging from the filter in the L-shaped runner system was the most stable among these systems. This appears to be because the flow directly impacts the filter in the U- and J-shaped systems, whereas the flow in the L-shaped system fills tangentially to the filter. Even without a filter, the flow in the L-shaped system was the most stable among the other systems.

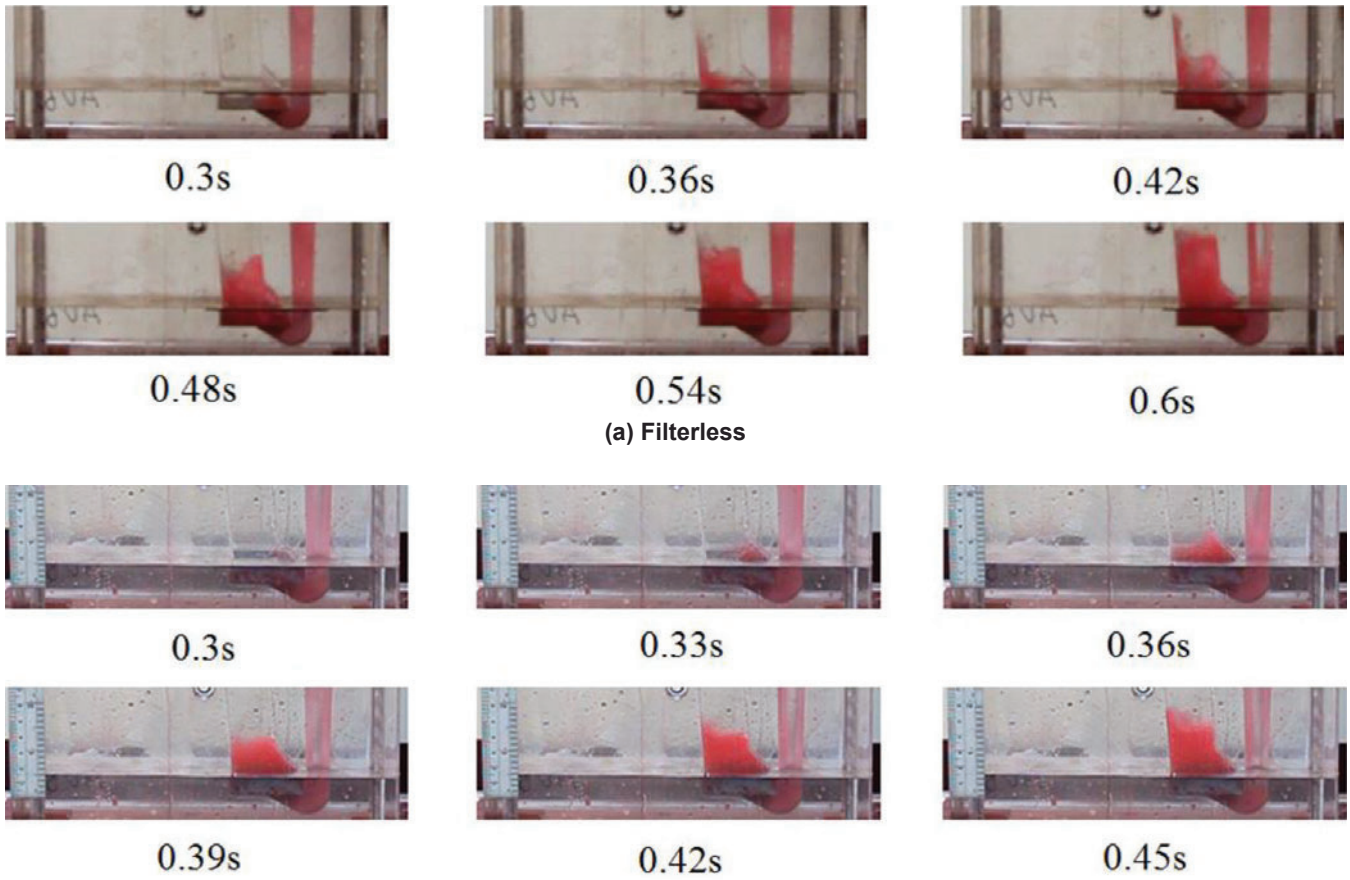

Figure 9. The water experiments for the J-shaped runner systems with: (a) filterless and (b) 10 ppi foam filter at the head height of 400mm in the various time frames.

Casting Experiments

It is now quite widely understood that if a casting is filled turbulently, the mutual impact of falling liquid metal and rising liquid metal (for instance) creates a submerged oxide-to-oxide interface; and a bifilm is formed. The creation of multiple unbonded double films in this way act as cracks in the liquid, but were often scrambled by internal bulk turbulence into compact convoluted forms. These compact bifilms were the normal form of crack-like defects in the solidified casting when frozen reasonably quickly. Such solidified castings have a bulk density very close to that of a degassed sample. However, if the casting is remelted and the external atmosphere pressure is reduced, the bifilm can become inflated by the gas from solution, unfolds and expands to become a pore.

Figure 10 shows the histograms of the volume percentages of porosities (ε) in the remelt RPT samples for the three runner systems at various head heights. In these samples, the volume of pores really depends on amount of soluble gas dissolved into the atomic structure during filling of liquid aluminum in the cavity. Because the content of the soluble gas of surrounding atmosphere in each pouring is random, it is difficult to read the difference among these systems by their porosities only.

Therefore, remelt RPT samples were sectioned across the center and ground with successively finer SiC papers to reveal porosities (Figure 11). It was logical to assume that each pore in the remelt RPT sample corresponds to an inflated bifilm.[10,11]

In Figure 11a, the bulk density of the original degassed sample, 2630 kg/m,[3] was measured. In order to investigate that the remelted samples were not picking up any additional humidity and gases during remelting in this study, the original degassed sample was remelted in the same procedure shown in the remelting process in the Casting Experiment Section of this paper. As a result, the equal density of this remelted sample (2630 kg/m^3) was also measured by wax sealed Archimedes method. It was proved that no extra gases were picked up during remelting process.

As the volume of the inflated bifilm or the pore is increasing, sometimes, the expanding bubble is eventually lost by bursting out from the surface of the solidifying specimen. A large stretched bifilm across the remelt RPT specimen in the filterless U400 system is shown in Figure 11c. Enclosed within this bifilm, there were several trapped bubbles. It is probable that this large bifilm was created from the observed turbulent fountain flow. As shown in Figure 8a, two large air bubbles

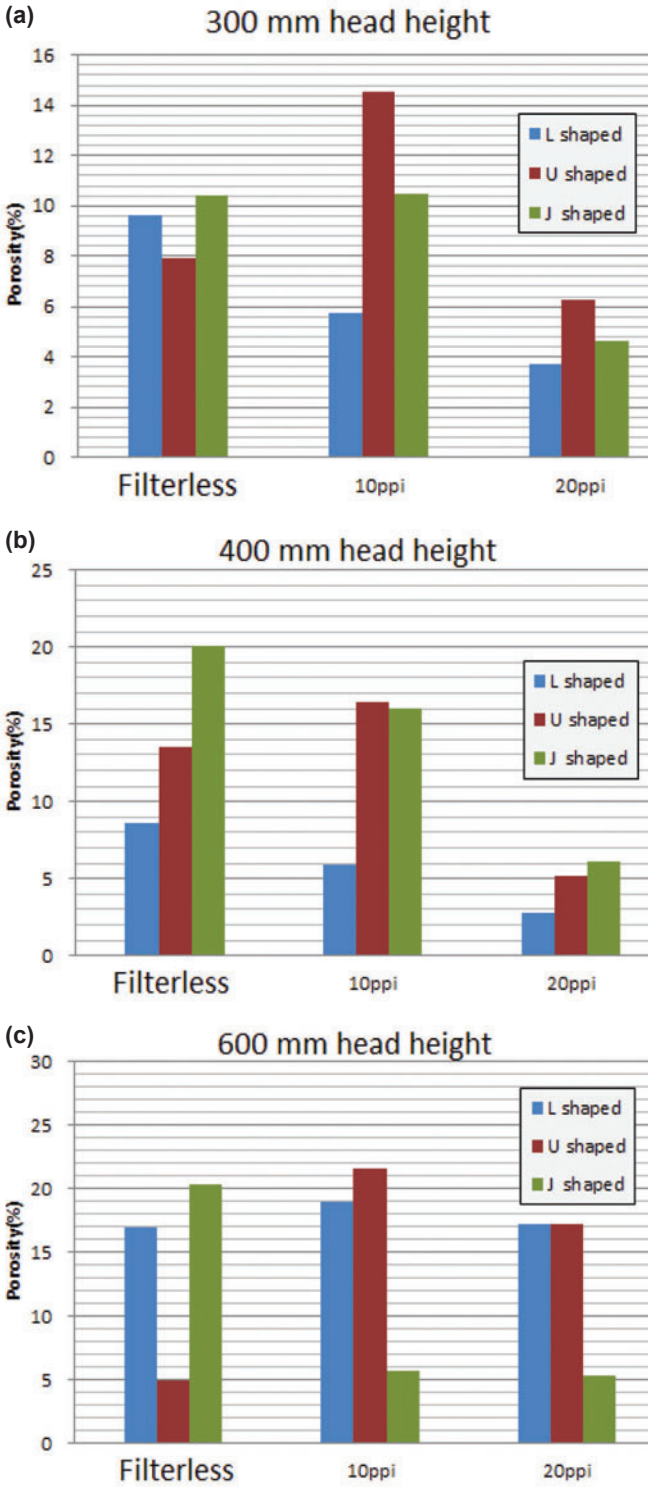

Figure 10. The volume percentages of porosity in the remelt RPT samples for the L-, U- and J- shaped runner systems at a head height of: (a) 300mm, (b) 400mm and (c) 600mm respectively.

were engulfed by the fountain. However, ultimately, the bubbles floated away but their trails, forming major bifilm defects, remained. The loss of large bubbles might explain why the volume percentage of the pores in this specimen is smaller (13.5%) than that in the U system with 10 ppi filter (16.5%). This large bifilm is a potentially dangerous defect in the casting.

Although there is no fountain-like flow in the 10 ppi filter U system, its sectioned specimen shows isolated inflated bi-films (i.e., 10 ppi, U400 in Figure 11c). It is also found that some inflated bi-films were trapped under the oxide film on the specimen surface. But, long bifilms, such as those shown in the filterless U400 system in Figure 11c, were not found in this system.

In the series of experiments on L400 systems (Figure 11b), the sectioned remelt RPT samples show that the pores were finer as the liquid aluminum passed through the finer filters. This may constitute evidence that the oxide bifilms were chopped into smaller sizes while passing through the filter as suggested by Sirrell and Campbell.[5] Similar results were shown in the series of experiments in J400 systems (Figure 11d).

As mentioned previously, it is difficult to tell the difference among these runner systems based on their porosity. This is because the content of the soluble gas in the surrounding atmosphere during each pour was not easy to control in the casting experiments. In this study, an "area normalized" bifilm index map was therefore introduced.

From all of the sectioned RPT samples shown in Figure 11, the contents of the bifilm defects were measured and the results were listed in Table 1. In this table the unit area (A_u) was 13mm × 13mm. The metal surface area on the unit area (A_m) is calculated from Equation 1.

Based on the results in Table 1, the bifilm index map which is the total length of bifilms per metal area as function of the number of bifilms for that area (three runner systems are shown in Figure 12). In each runner system without a filter (filterless condition), the total length of bifilms is about the same although various head heights were tested. For example; in L systems without a filter, the average L value was 0.10mm^{-1} (Figure 12a). That was an intrinsic creation of bifilms from this system and its total length of bifilm was a constant value. And, this value was independent on the head height. A high head height (e.g., 0-L600 Experiment) only resulted in developing a large piece of bifilm (e.g., N value was low for 0-L600 Experiment in Figure 12a).

For a 10 ppi foam filter in the L system, the L value increased from 0.08 to 0.21 mm^{-1} as the increased head height went from 300 to 600mm (i.e., route indicated by dashed arrows in Figure 12a). Similarly, for the 20 ppi foam filter in the L system, the L value increased with increasing head height. In a low head height such as 300mm, for these two filters, the L values were lower than the average value of 0.10 mm^{-1} in the filterless system. But at the high head height of 600mm, the L is much larger than the average value. This data implied that the filtration effect was only good for a low head height in an L-shaped system.

Table 1. Bifilm Measurements in Sectioned RPT Specimens

Filter System Head Height (ppi-system-mm)	Total Bifilm Length (L) (mm)	# of Bifilms, (N)	Porosity Volume % (ε)	Metal Surface Area on Unit Area (A_m) (%)	Total Length of Bifilm per A_m Area (L/A_m) (mm^{-1})	# of Bifilm per A_m Area (N/A_m) (mm^{-2})
0-L300	16.0	15	9.65	90.35	0.11	0.10
0-L400	15.5	14	8.64	91.36	0.10	0.09
0-L600	13.0	4	17.01	82.99	0.09	0.03
10-L300	12.0	10	5.72	94.28	0.08	0.06
10-L400	19.0	15	5.92	94.08	0.12	0.09
10-L600	29.0	13	18.95	81.05	0.21	0.10
20-L300	13.0	10	3.73	96.27	0.08	0.06
20-L400	20.0	12	2.76	97.24	0.12	0.07
20-L600	30.0	21	17.26	82.74	0.22	0.15
0-U300	21.0	16	7.88	92.12	0.14	0.10
0-U400	20.0	14	13.46	86.54	0.14	0.10
0-U600	21.0	15	4.95	95.05	0.13	0.09
10-U300	23.0	8	14.52	85.48	0.16	0.06
10-U400	29.0	12	16.45	83.55	0.21	0.09
10-U600	33.0	13	21.65	78.35	0.25	0.10
20-U300	19.0	12	6.30	93.70	0.12	0.08
20-U400	20.0	9	5.16	94.84	0.13	0.06
20-U600	18.7	4	17.21	82.79	0.13	0.03
0-J300	28.0	5	10.38	89.62	0.19	0.03
0-J400	26.0	5	20.10	79.90	0.19	0.04
0-J600	27.0	6	20.30	79.70	0.20	0.05
10-J300	23.0	9	10.49	89.51	0.15	0.06
10-J400	18.0	10	16.01	83.99	0.13	0.07
10-J600	18.0	13	5.68	94.32	0.11	0.08
20-J300	22.0	9	4.65	95.35	0.14	0.06
20-J400	21.0	17	6.10	93.90	0.13	0.11
20-J600	20.0	18	5.33	94.67	0.13	0.11

Moreover, the possible chopping effect took place at higher head heights for the 20 ppi filter. For instance, the N value increased from 0.06 to 0.15mm^{-2} as head height increased from 400 to 600mm, such as the route indicated by the dark arrows in Figure 12a. Both total length and number of bifilms increased as the head height increased. Consequently, in L-shaped system, the optimized head height of 300mm with foam filters is suggested.

In the U-shaped system, the average L value was 0.13mm^{-1} for a filterless condition (Figure 12b). For a 10 ppi foam filter in a U system, L value increased from 0.16 to 0.25mm^{-1} as the head height increased from 300 to 600mm (i.e., route indicated by the dashed arrows in Figure 12b). Compared to filterless U system, the 10ppi foam filter created long bifilms in the casting samples because their L values were greater than those in filterless systems and their N values were less than those in filterless systems. For an example, at a head height of 600mm (i.e., 10ppi U600 experiment), its N value was approximately equal to that in the filterless U system and L value was much larger than that in filterless system. It suggests that the bifilms in 10 ppi U600 system were the same numbers but longer lengths comparing to the filterless systems.

For 20 ppi foam filter in U system, the L values were lower than the average value of 0.13 mm^{-1} in the filterless system. L value increases from 0.12 to 0.13 mm^{-1} as increasing the head height from 300 to 600mm (i.e., the route indicated by dark arrows in Figure 12b). But at a high head height of 600mm, the L value went back to the average value in the filterless system. Also, N value decreased from 0.08 to 0.03 mm^{-2} as head height increased from 400 to 600mm. These results imply that the bifilms become longer as the head heights increased in the 20 ppi U system.

In all of the U systems, the total length of the bifilm was much greater than those of 10ppi-L300 and 20ppi-L300 systems (i.e., 0.08 and 0.08 mm^{-1} respectively). Filters in this system create large pieces of bifilm.

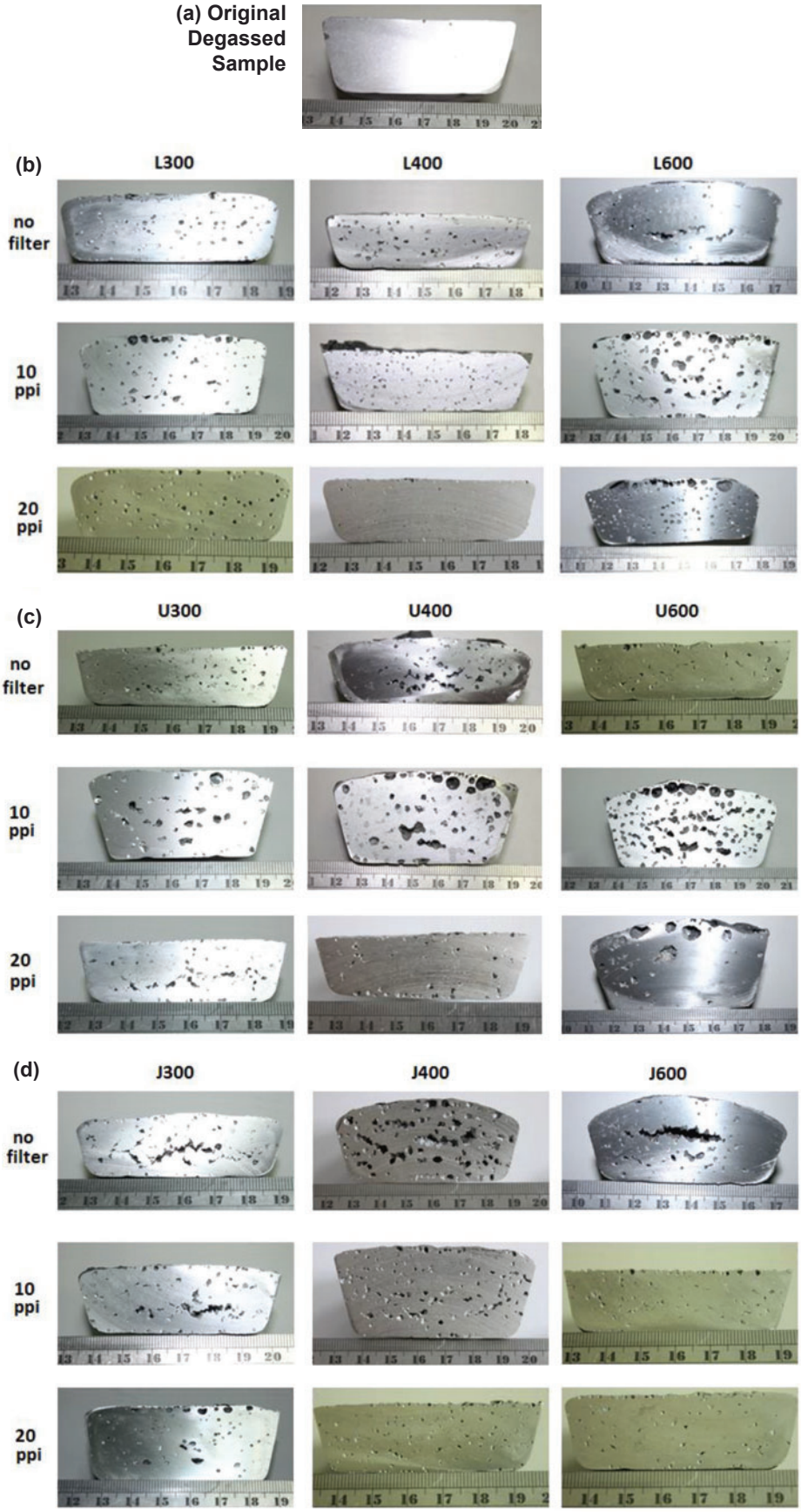

Figure 11. (a) The sectioned RPT specimens of the original liquid metal in the furnace after degassing; and the various re-melt RPT casting samples: (b) L-runner systems (c) U- runner system (d) J- runner system.

In the J-shaped system, the average of the L values was 0.19mm^{-1} for filterless condition (Figure 12c). For 10 ppi foam filter in a J system, L value decreased from 0.15 to 0.11 mm^{-1} as the head height increased from 300 to 600 mm (i.e., route indicated by the dashed arrows in Figure 12c). This indicates that the bifilms were chopped into shorter pieces and more bifilms were produced as head heights were increased. Similar results are shown in the 20 ppi J system as head heights increased (i.e., route indicated by the dark arrows in Figure 12c).

In the J system, filters were good for reducing the total length of bifilms, but they create some chopping effect for bifilms. Moreover, the total lengths of the bifilms in all of filtered J systems were still greater than those of the 10ppi-L300 and 20ppi-L300 systems.

Discussion

Based on the bifilm index map, the L300 systems with filters are suggested for future applications. However, it is not suggested to use filters if the effective head height is greater than 300mm. This is because both the numbers and total lengths of bifilms increase at the higher heads.

The "area normalized" index map is good for investigating the formation of bifilms during metal filling in runner systems. The lengths and numbers of bifilm were also related to the original cracks instituted in the solidified castings but not the gas contents. Therefore the total length of L values in the index map suggests the possibility of the start of crack propagation. The higher the value is the lower the mechanical property of the castings.

The average total length of bifilms in the filterless L system was the shortest (0.10 mm^{-1}) while the filterless J system was the longest (0.19 mm^{-1}). This suggests that L system intrinsically creates less bifilms among all systems. But the filters may damage the melt quality in L system with high heads. Sometimes, the filters in J systems may be good for reducing the length of bifilms although a chopped effect is inevitable. Filters in the U system may create longer pieces of bifilms.

Overall, the huge numbers of bifilms (or pores) generated simply by the melt "falling" into the various experimental systems is cause for concern. Clearly, the original melt in the furnace was of exceptionally high quality (Figure 11a), and this quality was immediately destroyed by

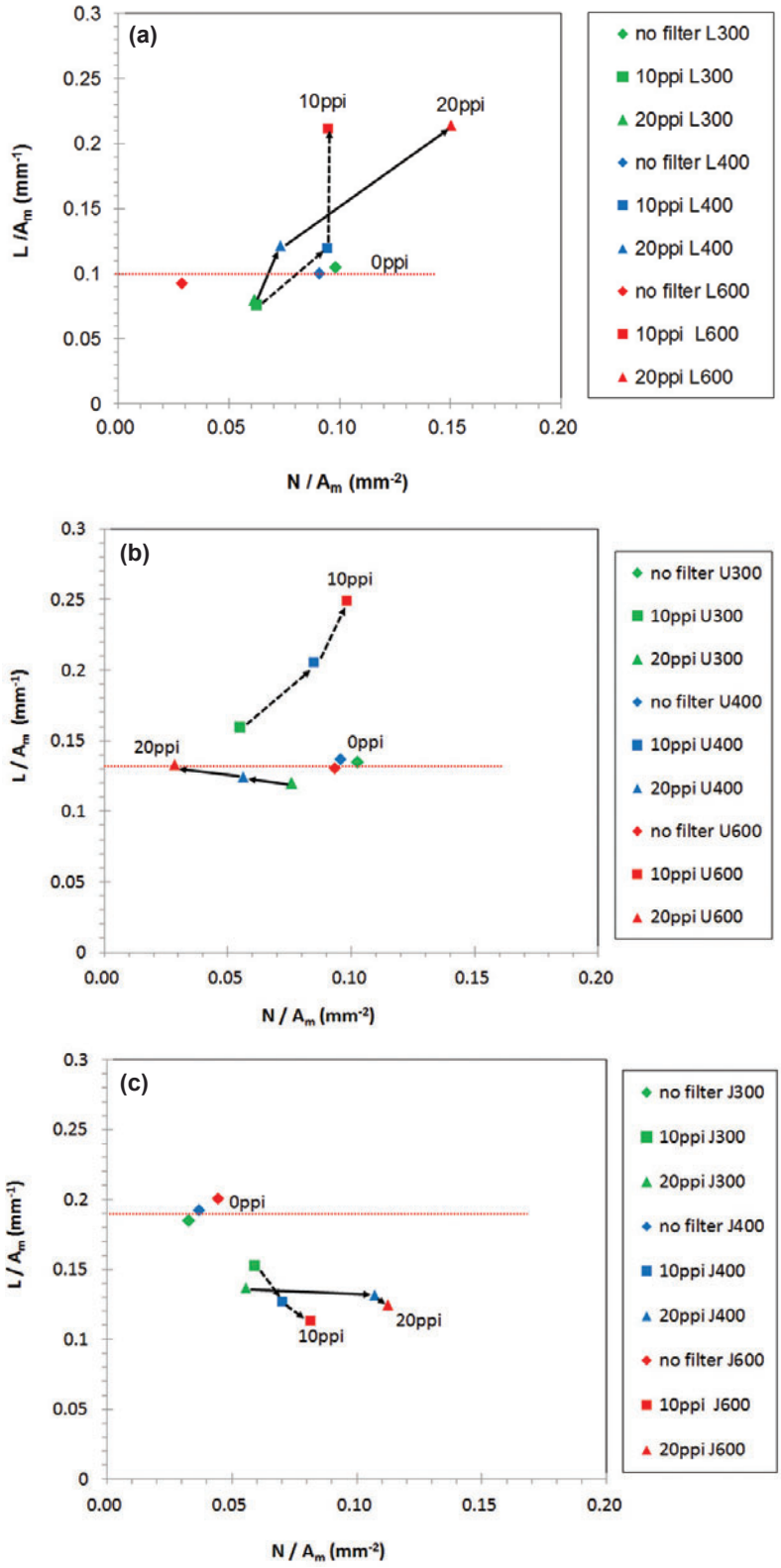

Figure 12. The "area normalized" bifilm index map for: (a) L-, (b) U-, and (c) J- shaped systems. (Noted that the red lines indicate the average L/A$_m$ values in the filterless condition for various head heights in the three systems.)

the act of pouring into the experimental casting. The immense damage caused by this relatively minor fall was a surprise, and should be an alarm signal to all metalcasters. The presence of the filter assisted in

stabilizing the subsequent flow, avoiding further creation of defects, but tended no so much to act as a filter, but probably acted more akin to an array of knives, chopping and slicing the bifilms to smaller sizes.

Clearly, in the case of both gravity systems, despite their modest falls under gravity, the damage caused by the falls is nowhere near reversed by the use of a filter. Perhaps a finer filter would have worked better, and this is intended to be investigated in a further phase of this work. Even so, in view of the scale of damage cause by the fall, one cannot be optimistic that the benefits of a finer filter would be great.

These results suggest a confirmation of the powerful advantage of counter-gravity filling systems for castings, in which the melt can be controlled at all time at speeds less than the critical 0.5 m/s, so that bifilm defects are never created, and the excellent quality of the original melt can be preserved into the resultant casting.

Conclusions

1. The "area normalized" bifilm index map was introduced to understand the lengths and numbers of bifilms created during filling the mold cavity. In this map, gas content was not the issue. Un-inflated bifilms are contained in solidified castings without pores. Large lengths and numbers of bifilms developed more sites for crack initiation and propagation.
2. The average total lengths of bifilms in the filterless L-, U- and J-shaped runner systems were: 0.10, 0.13 and 0.19 mm^{-1} respectively. L-systems intrinsically created fewer bifilms among all systems.
3. The L300 systems with filters are recommended for future applications. However, it is not suggested to use filters if the effective head height is greater than 300mm.
4. The use of filters in U-shaped runner systems creates longer bifilms. At a head height of 600mm (i.e., 10ppi U600 experiment), its N value was close to that in the filterless U system and L value was much greater than that in the filterless system. This suggests that the bifilms in the 10ppi U600 system were the same numbers but longer lengths compared to the filterless system. Similarly, the L values at various head heights in 20 ppi filter systems were close to the average total lengths of the filterless systems (0.13 mm^{-1}). Their N values decreased as the head heights increased. It also suggests that the larger bifilms were generated in this system.
5. The filters in the J system reduced the total length of bifilms, lengths were still greater than those in the filtered L300 systems. Conversely, the numbers of bifilms were increased, suggesting a chopping effect in the filtered J system.

Acknowledgements

F.-Y. Hsu acknowledges the sponsorship of Professor John Campbell and the help of Mr. Roger Kendrick, European Technology Manager Nonferrous Foundries, Foseco Europe, for providing the ceramic foam filters.

REFERENCES

1. Runyoro, J., Campbell, J., "The Running and Gating of Light Alloys," *The Foundryman*, pp. 117–124 (Apr. 1992).
2. Campbell, J., "Castings," p. 32, Oxford, Butterworth-Heinemann (1991).
3. Campbell, J., "The 10 Casting Rules: Guidelines for the Reliable Production of Reliable Castings; A Draft Process Specification, 1st Intl. Conference on Gating, Filling and Feeding of Aluminum Castings," American Foundry Society (AFS), Oct. 11–13, 1999, pp. 35–48 (1999).
4. Green, N.R., Campbell, J., "Statistical Distributions of Fracture Strengths of Cast Al-7Si-Mg," *Materials Science and Engineering*, vol. A173, pp. 261–266 (1993).
5. Sirrell, B., Campbell, J., "Mechanism of Filtration in Reduction of Casting Defects Due to Surface Turbulence during Mold Filling," *AFS Transactions,* vol. 105, pp. 645–654 (1997).
6. Hashemi, H., Raiszadeh, R., "Naturally-Pressurized Running Systems: The Role of Ceramic Filters," *Journal of Applied Sciences*, vol. 9, issue 11, pp. 2115–2122 (2009).
7. Gebelin, J.-C., Jolly, M.R., "Modelling Filters in Light Alloy Casting Processes (or "What Really Happens When Aluminium Flows Through a Filter")," *AFS Transactions*, vol. 110, pp. 109–119 (2002).
8. Hsu, F.-Y., Lin, H.-J., "Foam Filters Used in Gravity Casting," *Metallurgical and Materials Transactions B*, vol. 42, issue 6, pp. 1110–1117 (2011).
9. Din, T., Kendrick, R., Campbell, J., "Direct Filtration of A356 Alloy," *AFS Transactions*, vol. 111, pp. 91–100 (2003).
10. Campbell, J., "Castings," 2nd ed., Elsevier Science (May 29, 2003).
11. Dispinar, D., Campbell, J., "Shape Casting: 2nd International Symposium" Edited by Paul N. Crepeau, Murat Tiryakio–lu and John Campbell TMS (The Minerals, Metals & Materials Society), pp. 11–18 (2007).

Runner Systems Containing Ceramic Foam Filters Quantified By "Area Normalized" Bifilm Index Map

Fu-Yuan Hsu, Cheng-Lung Li
National United University, Miaoli City, Taiwan, R.O.C.

Reviewers: In addition to this work, it would be interesting to take controlled degassed samples and have them re-melted under the same experimental conditions as the excised samples to see how much of the porosity in the experimental samples is in fact due to bifilms formed during pouring and not due to the very act of re-melting the aluminum. It is possible in some conditions that the very act of re-melting the aluminum could be the source of some of the porosity evident in the pictured samples. Porosity due to re-melting and porosity due to bifilms during pouring should be differentiated in some way.

Authors: *The degassed sample was re-melted and the density of the re-melted sample is the same as the original sample. In Figure 11a, the bulk density of original degassed sample, 2630 kg/m^3, was measured. In order to investigate whether the re-melted samples were not getting additional humidity and gases during the re-melting processing in this study, the original degassed sample was re-melted in the same procedure shown in the re-melting process of Casting Experiment section. As a result, the equal density of this re-melted sample (2630 kg/m^3) was also measured by wax sealed Archimedes method. It was proved that no extra gases were picked up during re-melting process.*

Reviewers: Please provide a full description of how the excised samples were re-melted (e.g., in a muffle furnace? a small gas-fired crucible?) with a full description of the latent conditions (i.e., melting methodology, environmental conditions etc.).

Authors: *After casting, test samples were cut from the castings in the outlet area of the filter (denoted by the red rectangular region in Figure 4). The sectioned sample is approximately 170g (3cm×3cm×7cm) and it is contained in the RPT cup. The cup with the sample was re-melted at 1292±41°F (700±5°C) in an electric heated muffle furnace. The heating procedure is 50°F (10°C) per minute. At 1292±41°F (700±5°C), the cup with the re-melted sample stayed in the furnace for 1 hour before putting in the RPT vacuum. The cup then was transferred from the furnace and allowed its re-melted sample to re-solidify under vacuum (0.1 atmosphere residual pressures) in the RPT apparatus." This has been clarified in the final manuscript.*